Characterization of Layered γ-Titanium Phosphate $(C_2H_5NH_3)[Ti(H_{1.5}PO_4)(PO_4)]_2 \cdot H_2O$ Intercalate: A Combined NMR, Synchrotron XRD, and DFT Calculations Study

Luís Mafra* and João Rocha*

Department of Chemistry, CICECO, University of Aveiro, 3810-193 Aveiro, Portugal

Christian Fernandez

Laboratoire Catalyse et Spectrochimie (CNRS UMR 6506), ENSICAEN and Université de Caen-Basse Normandie, 14050 Caen, France

Germán R. Castro

SpLine, Spanish CRG Beamline, ESRF, BP 220, F-38043 Grenoble Cedex, France

Santiago García-Granda, Aranzazu Espina, Sergei A. Khainakov, and José R. García

Departamentos de Química Física y Analítica y Química Orgánica e Inorgánica, Universidad de Oviedo, 33006 Oviedo, Spain

Received January 17, 2008. Revised Manuscript Received March 7, 2008

Organically templated titanium phosphate, $(C_2H_5NH_3)[Ti(H_{1.5}PO_4)(PO_4)]_2 \cdot H_2O$, has been prepared by hydrothermal synthesis from titanium(IV) chloride, phosphoric acid, and ethylamine. The structure of this material has been characterized by synchrotron X-ray powder diffraction, ^1H, ^{13}C, ^{15}N, and ^{31}P (including $^1H\{FS\text{-}LG\}$-^1H HOMCOR, $^1H\{FS\text{-}LG\}$-^{31}P HETCOR, ^1H-^1H DQ-SQ, $^{13}C\{^{31}P\}$ REDOR) MAS NMR, and FTIR spectroscopies and thermal analyses (TG and DSC). Its triclinic structure was solved in the space group $P1$ (No. 1) with the following final unit cell parameters: $a = 5.1126(1)$, $b = 6.3189(2)$, $c = 12.0396(5)$ Å, $\alpha = 100.931(2)$, $\beta = 97.211(2)$, $\gamma = 90.683(3)°$, and $V = 378.62(2)$ Å^3 ($Z = 1$). This pseudo-three-dimensional compound is built up of anionic titanium phosphate layers, similar to those present in the γ-type titanium phosphate, and ethylammonium cations residing in the interlayer one-dimensional channels. On the basis of empirical (particularly NMR and powder XRD) and theoretical (DFT calculations using plane waves basis set) data, the ^1H NMR spectrum has been assigned, and evidence was found for a very strong interlayer P−O···H···O−P interaction.

Introduction

γ-Titanium phosphate compounds intercalated with *n*-alkylamine may be used as precursors in pillaring reactions, because of their water stability, suitable interlayer distance, moderate affinity of the intercalated species toward the host active centers, and an adequate occupied interlayer volume.[1–3] Despite the many potential applications of these materials,[4,5] their structural features have remained poorly understood. Recently, we have combined chemical information, NMR spectroscopy, powder XRD data, and chemical modeling studies to propose the first crystal structure of a *n*-alkylamine templated γ-titanium phosphate, $(C_6H_{13}NH_3)[Ti(HPO_4)(PO_4)] \cdot H_2O$.[6]

Although X-ray powder diffraction provides direct information on the crystal structure, it is not suitable to elucidate the local environment of ^1H nuclei. Probing ^1H environments is important to study intercalation compounds because of the presence of hydrogen bonding networks involving the guest molecules (alkylamine and water) and dihydrogenphosphate groups located on the surface of the γ-titanium phosphate layer. Solid-state NMR probes the local environment of a given nucleus and does not depend on the particle size or crystallinity of the material. Surprisingly, few NMR studies have been reported on γ-titanium phosphate intercalates,[6] except for the use of routine ^{31}P NMR to study the phosphate layer.[7]

Because of strong ^1H-^1H dipolar couplings, recording high-resolution ^1H NMR spectra of organic−inorganic hybrid

* Corresponding author. E-mail: lmafra@ua.pt.

(1) Menéndez, A.; Bárcena, M.; Jaimez, E.; García, J. R.; Rodríguez, J. *Chem. Mater.* **1993**, *5*, 1078.
(2) Espina, A.; Parra, J. B.; García, J. R.; Pajares, J. A.; Rodríguez, J. *Mater. Chem. Phys.* **1993**, *35*, 250.
(3) Espina, A.; Jaimez, E.; Khainakov, S. A.; Trobajo, C.; García, J. R.; Rodríguez, J. *Chem. Mater.* **1998**, *10*, 2490.
(4) Alberti, G.; Costantino, U. *Inclusion Compounds. Inorganic and Physical Aspects of Inclusion*; Oxford University Press: Oxford, 1991; Vol. 5.
(5) Alberti, G.; Casciola, M.; Costantino, U. *Adv. Mater.* **1996**, *8*, 291.
(6) Mafra, L.; Paz, F. A. A.; Rocha, J.; Espina, A.; Khainakov, S. A.; Garcia, J. R.; Fernandez, C. *Chem. Mater.* **2005**, *17*, 6287.
(7) Bortun, A.; Jaimez, E.; Llavona, R.; García, J. R.; Rodríguez, J. *Mater. Res. Bull.* **1995**, *30*, 413.

10.1021/cm800165p CCC: $40.75
Published on Web 05/24/2008

solids requires the use of fast MAS or MAS combined with certain multipulse shemes, employing the so-called CRAMPS techniques.[8–10]

Here we wish to report the hydrothermal synthesis and structural characterization of $(C_2H_5NH_3)[Ti(H_{1.5}PO_4)(PO_4)]_2 \cdot H_2O$, a new member of the layered γ-titanium phosphate family hosting ethylamine in the interlayer space, with pseudotridimensional porous structure and fibrous morphology, which shows unusual and very strong interlayer−hydrogen bonds. This material was characterized by a combination of one-dimensional (1D) and two-dimensional (2D) homo- and heteronuclear NMR methods, such as LG based ^{1}H decoupling schemes (^{1}H-^{1}H HOMCOR and ^{1}H-^{31}P HETCOR using FSLG and LG-CP homonuclear decoupling), fast MAS ^{1}H recoupling, and ^{13}C{^{31}P} rotational-echo double resonance (REDOR) spectroscopy. Molecular modeling studies, based on powder XRD, and calculation of the ^{1}H chemical shielding tensor values using density functional theory (DFT) are also reported.

Experimental Section

Synthesis. Hydrothermal synthesis of $(C_2H_5NH_3)[Ti(H_{1.5}PO_4)(PO_4)]_2 \cdot H_2O$ (yield >90%) was carried out in a stainless steel Teflon-lined vessel (designed and manufactured in the Oviedo University) under autogenous pressure. Ethylamine (Merck, solution 70% in water), 85% H_3PO_4 (Merck), and $TiCl_4$ (Merck, purity >99%) were mixed in molar ratios 1:10:10 ($TiCl_4$:H_3PO_4:$C_2H_5NH_2$) in a total volume of approximately 40 cm^3. The reaction vessel was sealed and heated to 185 °C for 10 days. The obtained solid was filtered off, washed with an excess of distilled water, and dried in air at ambient temperature.

Routine Characterization. The phosphorus and titanium contents were determined with a SpectraSpectrometer ICP-MS after dissolving a weighed amount of the sample in aqueous HF. Microanalytical data (C and N) were obtained with a Perkin-Elmer 2400B elemental analyzer. Thermal analyses were performed under nitrogen atmosphere (heating rate ca. 10 °C min^{-1}) in a Mettler-Toledo TGA/SDTA851^e and DSC822^e. Infrared spectra were recorded with a Perkin-Elmer 1000 FT-IR spectrophotometer using KBr pellets. Micrographs were recorded with a JEOL 2000EX-II transmission electron microscope, operating at 120−200 kV.

Diffraction Studies. Conventional X-ray powder diffraction patterns were collected on a diffractometer Philips 3040 with graphite-monochromatized Cu Kα radiation (λ = 1.5418 Å), operating in the Bragg−Brentano ($\theta/2\theta$) geometry. The sample was gently ground in an agate mortar, and the data were collected at ambient temperature over the angular range 3−90° 2θ, with a step of 0.02° and a counting time of 10 s/step. Indexing was performed independently with ITO12, TREOR90, and LZON, which are included in the CRYSFIRE suite.[11] Although a triclinic cell with a = 5.11, b = 6.32, c = 12.05 Å, and α = 100.9, β = 97.2, γ = 90.7° (M_{20} = 46) was found and both chemical composition and behavior suggest that their structure is related with the layered γ-titanium phosphate,[12] a structural solution was not reached.

Table 1. Crystal Data of $(C_2H_5NH_3)[Ti(H_{1.5}PO_4)(PO_4)]_2 \cdot H_2O$

formula	$C_2NO_{17}P_4Ti_2$
formula weight	529.71
crystal system	triclinic
space group	*P1* (No. 1)
a, Å	5.1126(1)
b, Å	6.3189(2)
c, Å	12.0396(5)
α, deg	100.931(2)
β, deg	97.211(2)
γ, deg	90.683(3)
V, Å^3	378.62(2)
Z	1
R_p	0.042
R_{wp}	0.056
R_{F^2}	0.083
χ	5.8

The synchrotron radiation powder diffraction pattern was recorded at beamline BM25A at the European Synchrotron Radiation Facility (ESRF), Grenoble (France). The sample was finely ground and loaded in a 1.0 mm diameter capillary. This capillary was mounted in a spinning goniometer. Room-temperature data were collected in a continuous 2θ-scan mode from 3° to 60° using an incident wavelength of 0.82648(6) Å (calibrated with NIST SRM 640c silicon powder; a = 5.4311946(92) Å).[13] The counts from the different channels were rebinned to produce an equivalent normalized step scan of 0.02° step intervals, with a count time of 5 s per step. Integrated intensities were extracted from the profile by using the Le Bail method[14] in the program GSAS.[15] Structure factors were extracted for 1303 reflections, of which 387 reflections were used for structure solution in the WINGX series of programs.[16] Direct methods SHELXS-97[17] in the space group *P*1 were successfully used to find the heavy atoms and two out of four P atoms. The positions of the remaining two P atoms were derived from the Patterson map on the basis of Ti−P interatomic vectors. No additional structural information could be derived from the structure factors extracted using the Le Bail method. Rietveld refinement of the pattern using the partial structural model as obtained above was carried out in the program GSAS. Initial least-squares refinements of the profile included terms for the scale factor, background, lattice parameters, zero point, and peak shape. A series of difference Fourier maps, computed at this stage, revealed peaks corresponding to the approximate positions of the remaining atoms in the structure. Residual electron density within the layers was assigned to the expected amine and water molecules. In addition to the peaks in the difference Fourier maps, it was necessary to use modeling techniques to obtain satisfactory geometries for the amine groups and water. Atomic positions were refined with soft constraints consisting of Ti−O, P−O, N−C, and C−C bond distances. During the final cycles of refinement, the weight for the soft constraints was reduced but could not be lifted completely for N−C and C−C bonds. The refinement of the positional parameters as well as their thermal parameters at this stage converged with R_{wp} = 0.056. The crystallographic data are given in Table 1, and the final Rietveld difference plot is given in Figure 1. Bond parameters are presented in Tables 2 and 3.

NMR Studies. ^{1}H, ^{13}C, ^{15}N, and ^{31}P spectra were recorded at 9.4 T on a Bruker Avance 400 wide-bore spectrometer (DSX model)

(8) Brown, S. P.; Spiess, H. W. *Chem. Rev.* **2001**, *101*, 4125.
(9) Rossum, B.-J. v.; Forster, H.; Groot, H. J. M. *J. Magn. Reson.* **1997**, *124*, 516.
(10) Vinogradov, E.; Madhu, P. K.; Vega, S. *Chem. Phys. Lett.* **1999**, *314*, 443.
(11) Shirley, R. *The CRYSFIRE System for Automatic Powder Indexing: User's Manual*; Lattice Press: Guildford, Surrey, U.K., 2000.
(12) Christensen, A. N.; Andersen, E. K.; Andersen, I. G. K.; Alberti, G.; Nielsen, M.; Lehmann, M. S. *Acta Chem. Scand.* **1990**, *44*, 865.
(13) National Institute of Standards and Technology, Department of Commerce (U.S.A.). http://www.nist.gov/srm. (accessed Nov 2007).
(14) Le Bail, A.; Duroy, H.; Fourquet, J. L. *Mater. Res. Bull.* **1988**, *23*, 447.
(15) Larson, A.; Von Dreele, R. B. *GSAS: Generalized Structure Analysis System*; Los Alamos National Laboratory: Los Alamos, NM, 1994.
(16) Farrugia, L. J. *J. Appl. Crystallogr.* **1999**, *32*, 837.
(17) Sheldrick, G. M. *SHELX97, Programs for Crystal Structure Analysis*, Release 97-2; University of Gottingen, Gottingen, Germany, 1997.

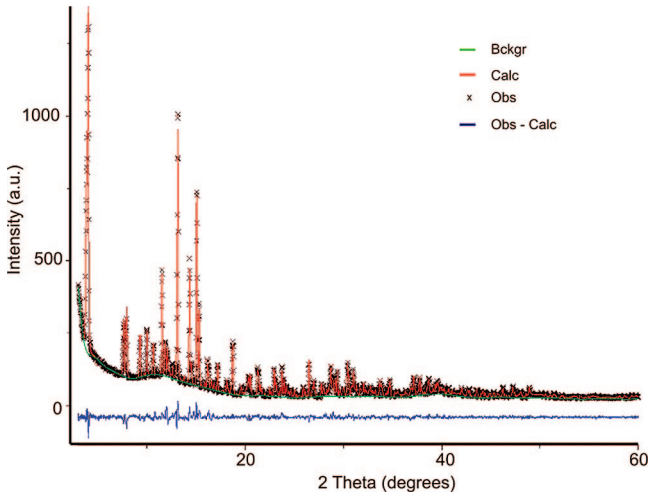

Figure 1. Synchrotron X-ray diffraction pattern of $(C_2H_5NH_3)[Ti(H_{1.5}PO_4)(PO_4)]_2 \cdot H_2O$. Observed (×), calculated (continuous line), background (line), and difference (below) profiles are plotted on the same scale.

on 4 mm (^{1}H, ^{13}C, and ^{31}P) and 7 mm (^{15}N) BL cross-polarization magic angle spinning (CPMAS) VTN probes at 400.1, 100.6, 161.9, and 40.5 MHz, respectively. The $^{13}C\{^{31}P\}$ REDOR experiment was recorded using a 4 mm triple-resonance probe. 2D NMR experiments using FS-LG homonuclear decoupling were carried out restricting the sample to the center of a 4-mm ZrO_2 rotor, with the help of two plastic inserts. This is necessary because the FS-LG decoupling step is sensitive to radiofrequency (rf) inhomogeneities and leads to an improvement of the rf field homogeneity over the whole volume of the sample. Efficient heteronuclear decoupling between ^{1}H and $^{13}C/^{31}P$ nuclei was achieved using the small phase incremental alternation with 64 steps (SPINAL64)[18] during the ^{13}C and ^{31}P acquisition in all experiments, which is a supercycle scheme consisting of a stepwise change in the phase angle of the TPPM sequence. A pulse length of 4.5 μs (ca. 165° pulses) was used for the basic unit of the SPINAL64 scheme, employing a ^{1}H rf field strength of $\nu_1^1H = 105$ kHz.

^{1}H MAS NMR. The settings are as follows: 90° excitation pulse of 2.5 μs; recycle delay, 10 s; and $\nu_R = 15-30$ kHz.

CPMAS NMR. The Hartmann−Hahn "sideband" condition $\nu_1^{13}C - \nu_1^1H = n\nu_R$ ($n = \pm1$, $n = \pm2$) was carefully matched by calibrating the ^{1}H and the X nutation frequencies (ν_1) during the contact time, where X = ^{13}C, ^{31}P, or ^{15}N.

^{13}C CPMAS NMR. The settings are as follows. $\nu_1^{13}C = 55$ kHz; $\nu_1^1H = 60-30$ kHz; recycle delay, 4 s; contact time, 1−2 ms; NS = 1k; $\nu_R = 12$ kHz. ^{31}P CPMAS NMR: $\nu_1^{31}P = 62.5$ kHz; $\nu_1^1H =$ 90 to 45 kHz; recycle delay, 4 s; contact time, 1−2 ms; NS = 16; $\nu_R = 12$ kHz. ^{15}N CPMAS NMR, $\nu_1^{15}N = 50$ kHz; $\nu_1^1H = 60$ to 30 kHz; recycle delay, 4 s; contact time, 4 ms; NS = 8k; $\nu_R = 5$ kHz. SPINAL-64 decoupling was used during data acquisition.

2D ^{1}H{FS-LG}-^{1}H/^{31}P HOMCOR/HETCOR NMR. The pulse sequences are described elsewhere.[9] Quadrature detection in t_1 was achieved by the States-TPPI method.[19] The ^{1}H chemical shifts and the scaling factor, λ, of the FS-LG dimension (F1) of HOMCOR/HETCOR spectra were determined by comparison with the 2D ^{1}H{FS-LG}-^{1}H HOMCOR spectrum, which shows well-resolved peaks, thus allowing the scaling factor for a given FS-LG rf field strength to be estimated. Scaling factors of 0.55−0.58 were obtained. Chemical shifts are quoted in parts per million (ppm) from tetramethylsilane (TMS) for the ^{1}H and ^{13}C nuclei, 85% H_3PO_4 for the ^{31}P, and glycine for ^{15}N.

2D ^{1}H DQ MAS. The back-to-back (BABA) recoupling sequence[20] was employed for the excitation and reconversion of DQ coherences (DQC). Two types of BABA sequences were used: the standard one (uncompensated version), using a recoupling time (τ_{rcpl}) synchronized with $1 \times \tau_R$, and its compensating variant employing $\tau_{rcpl} = 2 \times \tau_R$. The former sequence takes the form $\Delta/2 - \phi_x - \tau - \phi_{-x} - \Delta - \phi_y - \tau - \phi_{-y} - \Delta/2$, while the latter takes the form $\Delta/2 - \phi_x - \tau - \phi_x - \Delta - \phi_y - \tau - \phi_{-y} - \Delta - \phi_x - \tau - \phi_x - \Delta - \phi_{-y} - \Delta - \phi_y - \Delta/2$, where $\phi_i\{i = x,-x,y,-y\}$ is the phase of each rf pulse with a 90° flip angle and $\Delta = 2$ μs denotes

Table 2. Selected Bond Lengths (Å) and Angles (deg) of $(C_2H_5NH_3)[Ti(H_{1.5}PO_4)(PO_4)]_2 \cdot H_2O$

Ti(1)−O(1)	1.90(3)	O(2)−Ti(2)−O(15)	89.7(13)
Ti(1)−O(4)	2.01(3)	O(2)−Ti(2)−O(16)	177.5(15)
Ti(1)−O(7)	1.94(4)	O(3)−Ti(2)−O(10)	87.5(13)
Ti(1)−O(8)	1.90(4)	O(3)−Ti(2)−O(12)	90.4(13)
Ti(1)−O(9)	1.89(4)	O(3)−Ti(2)−O(15)	175.8(14)
Ti(1)−O(11)	1.88(3)	O(3)−Ti(2)−O(16)	84.7(13)
Ti(2)−O(2)	1.82(4)	O(10)−Ti(2)−O(12)	177.8(14)
Ti(2)−O(3)	1.97(4)	O(10)−Ti(2)−O(15)	90.4(13)
Ti(2)−O(10)	1.90(3)	O(10)−Ti(2)−O(16)	90.4(14)
Ti(2)−O(12)	2.04(3)	O(12)−Ti(2)−O(15)	91.7(12)
Ti(2)−O(15)	2.11(3)	O(12)−Ti(2)−O(16)	88.8(13)
Ti(2)−O(22)	1.93(3)	O(15)−Ti(2)−O(16)	91.7(13)
P(1)−O(1)	1.58(4)	Ti(1)−O(1)−P(1)	140.6(23)
P(1)−O(2)	1.62(4)	Ti(1)−O(4)−P(1)	135.2(18)
P(1)−O(3)	1.39(3)	Ti(1)−O(7)−P(3)	166.7(24)
P(1)−O(4)	1.57(4)	Ti(1)−O(8)−P(3)	149.9(25)
P(2)−O(9)	1.53(4)	Ti(1)−O(9)−P(2)	160.9(21)
P(2)−O(10)	1.54(4)	Ti(1)−O(11)−P(2)	146.3(20)
P(2)−O(11)	1.59(3)	Ti(2)−O(2)−P(1)	164.2(21)
P(2)−O(12)	1.46(3)	Ti(2)−O(3)−P(1)	156.7(24)
P(3)−O(5)	1.39(3)	Ti(2)−O(10)−P(2)	144.4(22)
P(3)−O(6)	1.74(2)	Ti(2)−O(12)−P(2)	142.0(22)
P(3)−O(7)	1.48(4)	Ti(2)−O(15)−P(4)	128.4(15)
P(3)−O(8)	1.61(4)	Ti(2)−O(16)−P(4)	159.5(23)
P(4)−O(13)	1.61(3)	O(1) −P(1)−O(2)	108.7(20)
P(4)−O(14)	1.68(2)	O(1)−P(1)−O(3)	118.8(22)
P(4)−O(15)	1.53(3)	O(1) −P(1)−O(4)	101.3(19)
P(4)−O(16)	1.46(4)	O(2) −P(1)−O(3)	108.8(21)
N(1)−C(1)	1.47(1)	O(2) −P(1)−O(4)	106.1(18)
C(1)−C(2)	1.53(1)	O(3) −P(1)−O(4)	112.2(20)
		O(9)−P(2)−O(10)	107.0(19)
N(1)−C(1)−C(2)	111.6(29)	O(9)−P(2)−O(11)	109.8(19)
O(1)−Ti(1)−O(4)	176.7(16)	O(9)−P(2)−O(12)	114.4(22)
O(1)−Ti(1)−O(7)	91.3(15)	O(10)−P(2)−O(11)	110.(2)
O(1)−Ti(1)−O(8)	84.8(13)	O(10)−P(2)−O(12)	106.0(21)
O(1)−Ti(1)−O(9)	91.4(13)	O(11)−P(2)−O(12)	109.5(20)
O(1)−Ti(1)−O(11)	89.3(14)	O(5)−P(3)−O(6)	117.4(19)
O(4)−Ti(1)−O(7)	87.6(12)	O(5)−P(3)−O(7)	109.9(21)
O(4)−Ti(1)−O(8)	92.2(13)	O(5)−P(3)−O(8)	111.1(21)
O(4)−Ti(1)−O(11)	93.8(13)	O(6)−P(3)−O(7)	103.9(18)
O(7)−Ti(1)−O(8)	87.2(15)	O(6)−P(3)−O(8)	105.7(16)
O(7)−Ti(1)−O(9)	173.8(17)	O(7)−P(3)−O(8)	108.3(20)
O(7)−Ti(1)−O(11)	94.3(15)	O(13)−P(4)−O(14)	110.5(16)
O(8)−Ti(1)−O(9)	87.5(15)	O(13)−P(4)−O(15)	107.4(16)
O(8)−Ti(1)−O(11)	173.9(13)	O(13)−P(4)−O(16)	117.5(19)
O(9)−Ti(1)−O(11)	91.3(15)	O(14)−P(4)−O(15)	109.2(14)
O(2)−Ti(2)−O(3)	93.8(15)	O(14)−P(4)−O(16)	106.4(19)
O(2)−Ti(2)−O(10)	87.5(14)	O(15)−P(4)−O(16)	105.5(19)
O(2)−Ti(2)−O(12)	93.2(13)		

Table 3. Short (N,O)···O Contacts (Å) in $(C_2H_5NH_3)[Ti(H_{1.5}PO_4)(PO_4)]_2 \cdot H_2O$

N(1)···O(10)	3.46	N(1)···O(14)	3.34
N(1)···O(12)	3.49	O(5)···O(13)	2.43
N(1)···O(13)	3.53	O(W)···O(6)	1.60

(18) Fung, B. M.; Khitrin, A. K.; Ermolaev, K. *J. Magn. Reson.* **2000**, *142*, 97.
(19) Marion, D.; Ikura, M.; Tschudin, R.; Bax, A. *J. Magn. Reson.* **1989**, *85*, 393.
(20) Feike, M.; Demco, D. E.; Graf, R.; Gottwald, J.; Hafner, S.; Spiess, H. W. *J. Magn. Reson., Ser. A* **1996**, *122*, 214.

Scheme 1

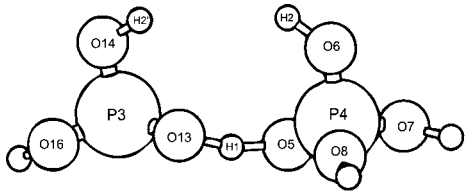

$[(H_3PO_4)(H_2PO_4)]^-$

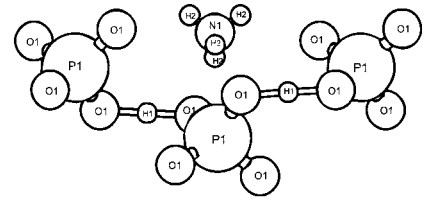

$NH_4H_2PO_4$

the interpulse delay to allow time for phase switching, thus avoiding pulse errors coming from consecutive pulses. The delay τ equals $\tau_R/2$, subtracting the contribution of the two adjacent pulse lengths and two times $\Delta/2$. The careful synchronization of the sequence is necessary for best ^{1}H homonuclear recoupling. A final reading 90° pulse, followed by a *z*-filter delay (integer number of the rotor period), creates transversal magnetization. Sign discrimination during the t_1 evolution was attained using TPPI[21] or States[22] acquisition.

^{13}C Relaxation. T_1^C and $T_{1_\rho}^C$ were measured with the Torchia sequence[23] and a variable spin-lock pulse length on the ^{13}C channel after a CP transfer, respectively. The spin-lock power level employed for both strategies was the same as described above for CPMAS. For T_1^C measurements, the variable delay was incremented in 22 steps: 5, 10, 20, 30, 60, 80, 100, 150, 200, 300, 350, 400, 500, 700, 1000, 3000, 5000, 7000, 15000, 25000, 50000, and 100000 ms. For $T_{1_\rho}^C$ measurements, the variable spin-lock pulse duration was incremented in 10 steps: 60, 80, 90, 100, 130, 150, 200, 250, and 300 ms. The obtained curves were fitted with monoexponential functions.

$^{13}C\{^{31}P\}$ REDOR. REDOR was employed to reintroduce the dipolar couplings, between coupled heteronuclear spin pairs, that are removed by magic-angle spinning.[24] REDOR experiments are always performed in two parts: with (S) and without (full echo, S_0) rotor-synchronized dephasing pulses. The dephasing pulses change the sign of the heteronuclear dipolar coupling, and this interferes with the spatial averaging resulting from the sample spinning. The difference in the signal intensity (REDOR difference, $\Delta S = S_0 - S$) for the observed spin in the two parts of the REDOR experiment is directly related to the corresponding distance to the dephasing spin. $^{13}C\{^{31}P\}$ REDOR curves are plots of the fraction ($\Delta S/S_0$) against the number of rotor periods (NcT_R) where each ^{31}P 180° dephasing pulse is applied during a half-rotor period. These ^{31}P pulses affect the observed ^{13}C signal by preventing rotational refocusing of the dipolar interaction, leading to an experiment, *S*, where the ^{13}C resonance intensities decrease as the number of ^{31}P π pulses increases. Subtracting the *S* experiment from a second identical experiment, S_0, where for this time ^{31}P π pulses are not applied, we obtain a REDOR difference, ΔS , where the change in signal intensity is related to the distance between the coupled spins. Then, considering an isolated spin pair such strategy works well and has been widely used to measure distances between many different spin pairs. In particular $^{13}C-^{31}P$ REDOR has been mostly used to measure $^{13}C-^{31}P$ distances in biological samples.[25,26] To eliminate resonance offset effects, the $^{13}C\{^{31}P\}$ REDOR spectra were collected with standard xy-8 phase cycling, on the ^{31}P dephasing channels.[27] The REDOR experimental conditions used are 90° ^{1}H rf pulse, 4.5 μs; 180° ^{13}C rf pulse length, 11 μs (46 kHz); 180° ^{31}P rf pulse length, 10.4 μs (48 kHz); $\nu_R = 7$ kHz; the CT for CP transfer, 1.6 ms; ^{1}H decoupling during t_2, $\nu_1^1H = 78$ kHz.

Theoretical Calculations. Quantum mechanical calculations were performed using a first-principles approach involving no adjustable parameters based on density functional theory (DFT), as implemented in the program CASTEP.[28] Calculations of ^{1}H NMR chemical shifts were performed with the gauge-including projector augmented-wave method (GIPAW) developed by Pickard and Mauri.[29] Plane waves were used as the basis functions and the exchange and correlation energies of the electrons handled by the generalized gradient approximation (GGA). Several kinetic energy cutoffs (390−610 eV) and "on the fly" (OTFG) pseudopotentials were used to compute the magnetic shielding properties.

Initially, geometry optimizations were performed with fixed lattice parameters and internal coordinates for P atoms and full relaxation of internal coordinates for the other atoms (convergence criteria for the total energy: 10^{-6} eV atom^{-1}). Next, energy calculations with computing NMR chemical shielding were performed. The calculations with different cutoffs and number of Monkhorst-Pack *k*-points grid, sufficient to achieve convergence,[30] were performed on $[(H_3PO_4)(H_2PO_4)]^-$ and $NH_4H_2PO_4$ molecular units (Scheme 1).

The theoretical ^{1}H NMR chemical shifts depicted in Table 4 were calculated as the differences of isotropic shielding constants and the isotropic chemical shielding of the ^{1}H reference molecule (TMS, $\sigma_{iso} = 30.8$ ppm), also calculated in this work by the same method.

Table 4. Experimental and Theoretical ^{1}H Chemical Shifts (in ppm) for the Titled Material $[(C_2H_5NH_3)[Ti(H_{1.5}PO_4)(PO_4)]_2 \cdot H_2O]$ and the $[(H_3PO_4)(H_2PO_4)]^-$ and $NH_4H_2PO_4$ Units, Respectively

	experimental	calculated[a]	
^{1}H species	$(C_2H_5NH_3)[Ti(H_{1.5}PO_4)(PO_4)]_2 \cdot H_2O$	$[(H_3PO_4)(H_2PO_4)]^-$	$NH_4H_2PO_4$
PO···HA···OP	16.2	18.2	15.3
P-OH[B,C]	9.4, 7.6	8.1	
N-H[D]	6.8		5.3

[a] The theoretical ^{1}H NMR chemical shifts (δ_{iso}) are calculated as the differences between the isotropic shielding constants (σ_{iso}) with the isotropic chemical shielding of the ^{1}H reference molecule, TMS, using a σ_{iso}(TMS) = 30.8 ppm (obtained in this work and in agreement with the bibliographic data: 30.6−31.7 ppm).[37] For the $[(H_3PO_4)(H_2PO_4)]^-$ molecular unit, H1 and H2 correspond to the PO···(H1)···OP and PO(H2) proton, while in $NH_4H_2PO_4$ H1 and H2 they correspond to PO···(H1)···OP and N(H2) proton environments, respectively.

Results and Discussion

The first (and dominant) low-angle reflection of the powder XRD pattern of the title compound appears at a *d*-spacing

(21) Marion, D.; Wuthrich, K. *Biochem. Biophys. Res. Commun.* **1983**, *113*, 967.
(22) States, D. J.; Haberkorn, R. A.; Ruben, D. J. *J. Magn. Reson.* **1982**, *48*, 286.
(23) Torchia, D. A. *J. Magn. Reson.* **1978**, *30*, 613.
(24) Gullion, T.; Schaefer, J. *Adv. Magn. Reson.* **1989**, *13*, 58.
(25) Christiensen, A. M.; Schaefer, J. *Biochemistry* **1993**, *32*, 2868.
(26) Doherty, T.; Waring, A. J.; Hong, M. *Biochemistry* **2006**, *45*, 13323.
(27) Gullion, T.; Baker, D. B.; Conradi, M. S. *J. Magn. Reson.* **1990**, *89*, 479.
(28) Clark, S. J.; Segall, M. D.; Pickard, C. J.; Hasnip, P. J.; Probert, M. J.; Refson, K.; Payne, M. C. *Z. Kristallogr.* **2005**, *220*, 567.
(29) Pickard, C. J.; Mauri, F. *Phys. Rev.* **2001**, *B63*, 245101.
(30) Monkhorst, H. J.; Pack, J. D. *Phys. Rev. B* **1976**, *13*, 5188.

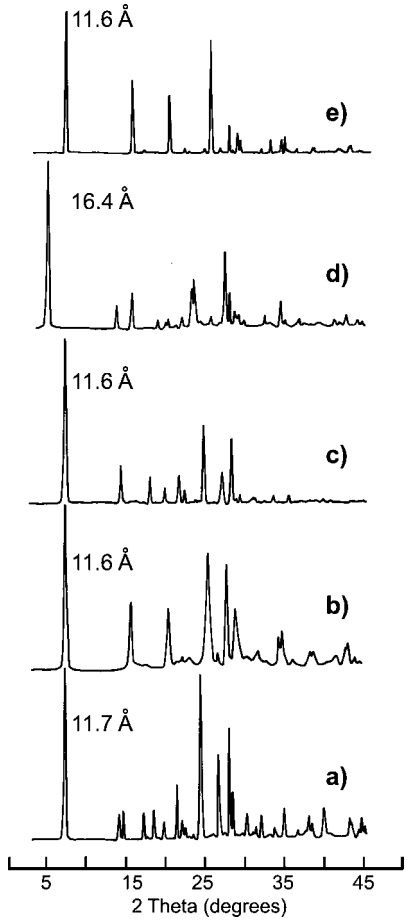

Figure 2. Powder XRD patterns of $(C_2H_5NH_3)[Ti(H_{1.5}PO_4)(PO_4)]_2 \cdot H_2O$: (a) as synthesized, (b) treated with 0.1 M HNO_3, (c) treated at 200 °C, and (d) stabilized at room temperature in a saturated atmosphere of ethylamine for 12 h. For comparison, the simulated powder XRD pattern of γ-titanium phosphate, $Ti(H_2PO_4)(PO_4) \cdot 2H_2O$, is shown in (e).

of approximately 11.7 Å (Figure 2a). Treatment of this compound with mineral acids (e.g., 0.1 M HNO_3) yields γ-titanium phosphate, $Ti(H_2PO_4)(PO_4) \cdot 2H_2O$ (Figure 2b), indicating that the inorganic matrices of the material and γ-layered titanium phosphate are similar.[6] According to elemental composition and thermal analyses (Table 5), this new titanium phosphate may be formulated as $(C_2H_5NH_3)[Ti(H_{1.5}PO_4)(PO_4)]_2 \cdot H_2O$ empirical formula. We note that when ethylamine ($C_2H_5NH_2$) inclusion occurs, there is proton transfer from the acidic hydrogenophosphate moieties in the γ-titanium phosphate layers to the amine group, thus leading to the presence of ethylammonium cations ($C_2H_5NH_3^+$) in the interlayer spaces (evidenced by solid-state NMR studies, see below).

Thermogravimetry gives a total weight loss from ambient temperature to 1000 °C of approximately 18.0% (Figure S1, Supporting Information), consistent with a TiP_2O_7 residue (calculated 18.2%). DTG and DSC curves show that the thermal decomposition process takes place with two steps. The first weight loss, at 40−150 °C, corresponds to the release of a water molecule per formula unit (observed ca. 3.3%, calculated 3.3%). The following weight loss (at a temperature in excess of 300 °C) corresponds to sequential removal of ethylamine and structural water from the condensation of hydrogenphosphate groups (observed ca. 14.7%, calculated 14.9%). The dehydration is a reversible process, and the water is zeolitic (heating the sample at approximately 200 °C followed by their stabilization in air does not change the powder XRD pattern nor the elemental analysis, Table 5). The corresponding decomposition route is shown below.

$$(C_2H_5NH_3)[Ti(H_{1.5}PO_4)(PO_4)]_2 \cdot H_2O(s) \leftrightarrows (C_2H_5NH_3)[Ti(H_{1.5}PO_4)(PO_4)]_2(s) + H_2O(g)$$

$$(C_2H_5NH_3)[Ti(H_{1.5}PO_4)(PO_4)]_2(s) \rightarrow 2TiP_2O_7(s) + C_2H_5NH_2(g) + 2H_2O(g)$$

The FTIR spectrum of the title material (Figure S2, Supporting Information) exhibits O−H stretching and H−O−H bending vibrations. The strong bands at 3611 and 3546 cm^{-1} are assigned to (ν) O−H and (ν) P−O−H stretching vibrations, while the band at 1617 cm^{-1} corresponds to the in-plane (δ_s) H−O−H deformation vibrational modes. Moreover, the intense bands at approximately 1220 cm^{-1} are attributed to the stretching mode in the plane of the P−O−H bonds or to the presence of water molecules adsorbed on phosphate layers. The *n*-ethylammonium cations give the symmetric (ca. 3009 cm^{-1}) and antisymmetric (ca. 2987, 2944 cm^{-1}) stretching (ν) modes of the $-CH_2-$ alkyl chains, and also the bands at approximately 1560 cm^{-1} are attributed to the N−H in-plane deformation (δ_s), while the bands at 3284 and 3144 cm^{-1} are assigned to, respectively, stretching (ν) N−H asymmetric and symmetric vibrations of the protonated amine group. The $-CH_2-$ groups also display a sharp scissoring (νs) band near 1400 cm^{-1}. A broad band at 900−1200 cm^{-1} corresponds to the stretching and bending vibrations of the P−O bonds.

Structure Description of $(C_2H_5NH_3)[Ti(H_{1.5}PO_4)(PO_4)]_2 \cdot H_2O$. When the elongated homogeneous size plates of $(C_2H_5NH_3)[Ti(H_{1.5}PO_4)(PO_4)]_2 \cdot H_2O$ (Figure S3, Supporting Information) are stored in an atmosphere saturated with ethylamine, a new crystalline phase with an interlayer distance of approximately 16.4 Å is isolated (Figure 2d), and the intercalation process occurs smoothly with no particle morphology change. This *d*-spacing was previously observed in a material obtained by solid−vapor contact of γ-titanium phosphate with *n*-ethylamine, $(C_2H_5NH_3)[Ti(HPO_4)(PO_4)] \cdot 0.3(C_2H_5NH_2) \cdot H_2O$,[1] and elemental composition studies (Table 5) confirm the presence of the same phase.

The structure of γ-titanium phosphate and previously reported $(C_6H_{13}NH_3)[Ti(HPO_4)(PO_4)] \cdot H_2O$[6] are related.[12] In this intercalation compound, individual two-dimensional anionic $[Ti(HPO_4)(PO_4)]^-$ sheets are constructed by corner-sharing four-ring chains formed by $\{PO_4\}$ tetrahedra and $\{TiO_6\}$ octahedra.[6] The structure contains two kinds of phosphate groups: PO_4^{3-} sharing their oxygen atoms with titanium centers and HPO_4^{2-} having two bridging and two terminal oxygen atoms. These terminal HPO_4^{2-} groups are connected to the chains and point toward the interlayer region, directly interacting with the protonated amine groups from neighboring *n*-hexylammonium cations through hydrogen bonding. In the titled compound, the inorganic layer arrangement is topologically similar to that in γ-titanium phosphate (Figure 3a,c). However, the Ti−O, P−O, O−Ti−O,

Table 5. Analytical Data and Weight Loss at 800 °C for Intercalation Compounds

formula	experimental (in %)					calculated (in %)						
	Ti	P	C	H	N	weight loss	Ti	P	C	H[a]	N	weight loss
$(C_2H_5NH_3)[Ti(H_{1.5}PO_4)(PO_4)]_2\cdot H_2O$[b]	17.4	22.6	4.4	1.9	2.5	18.0	17.7	22.8	4.4	2.4(0.6)	2.6	18.2
$(C_2H_5NH_3)[Ti(H_{1.5}PO_4)(PO_4)]_2\cdot H_2O$[c]	17.5	22.5	4.4	1.8	2.4	17.9	17.7	22.8	4.4	2.4(0.6)	2.6	18.2
$(C_2H_5NH_3)[Ti(HPO_4)(PO_4)]\cdot 0.3\ C_2H_5NH_2\cdot H_2O$[d]	15.0	19.2	9.7	3.7	5.8	29.7	15.1	19.5	10.1	3.9(0.3)	5.9	30.2

[a] In brackets, percentage of recalcitrant hydrogen (dihydrogenphosphate groups). [b] Sample obtained by hydrothermal synthesis and stabilization at room temperature or later. [c] Thermally treated (1 day) at 200 °C and stabilization in air at room temperature. [d] Obtained by solid−vapor contact of starting sample with ethylamine (12 h).

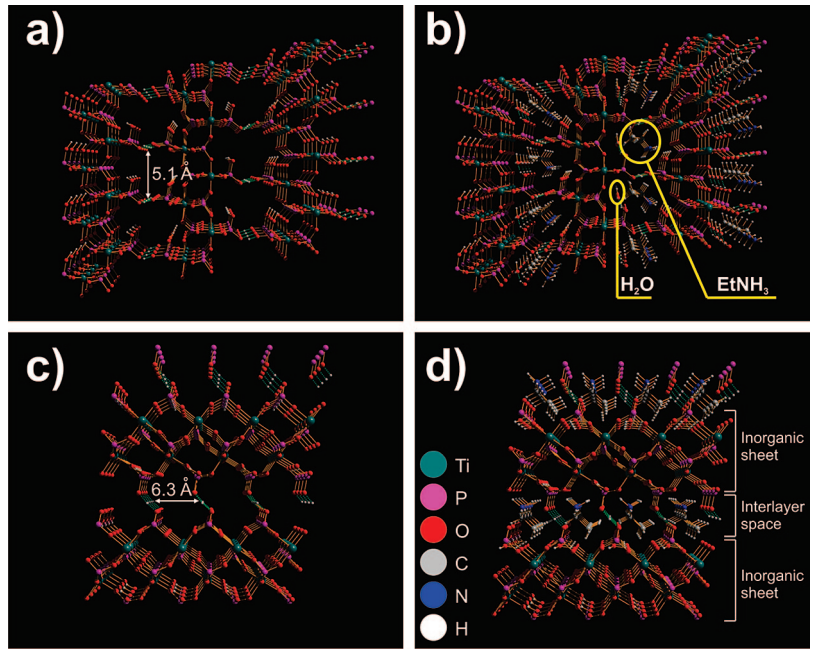

Figure 3. Perspective view of $(C_2H_5NH_3)[Ti(H_{1.5}PO_4)(PO_4)]_2\cdot H_2O$ crystal structure: two-dimensional anionic inorganic sheet and the interlayer space viewed along (a, b) the *a*-axis and along (c, d) the *b*-axis; (a, c) omitting and (b, d) showing water molecules and ethylammonium cations. Hydrogen bondings are represented as green dotted lines. The ^1H-^1H distances between adjacent POH groups involved in interlayer strong hydrogen bondings are depicted in (a) and (c). The guest species are indicated by yellow circles in (b), and the legend of colors is shown in (d).

and O−P−O bond lengths and angles (Table 2) are typical of other reported titanium phosphates.[31,32] Inspection of hydrogen bond contacts (Table 3) reveals short O−O distances, O(5)−O(13) = 2.43 Å, suggesting the existence of an unusual interlayer P−O···H···O−P hydrogen bond,[33] shown by 2D ^1H NMR and DFT calculations to be very strong. Therefore, the size and amount of intercalated amine lead to a strong interaction between adjacent inorganic layers, originating a negatively charged pseudo-3D structure, $[(O_4P)Ti(HO_3PO)\cdots H\cdots(OPO_3H)Ti(PO_4)]^-$, containing two types of 1D channels, whose interconnection generates a tunnel 2D network, housing ethylammonium cations and water molecules (Figures 3b,d and 4).

Synchrotron X-ray powder diffraction gives direct information on the crystal structure but does not elucidate, in detail, the local hydrogen atom environments, something ^1H NMR is well suited to do.

Solid-State NMR. The ^{13}C and ^{15}N CPMAS NMR spectra (Figure S4, Supporting Information) of the title material show the presence of a single crystallographically nonequivalent ethylamine guest molecule in the asymmetric unit. The ^{13}C CPMAS spectrum exhibits peaks at approximately 38.6 and 15.2 ppm attributed to, respectively, $N-CH_2$ and CH_3 groups, while the ^{15}N CPMAS spectrum shows a single peak at approximately −343 ppm, typical of protonated amines.[34]

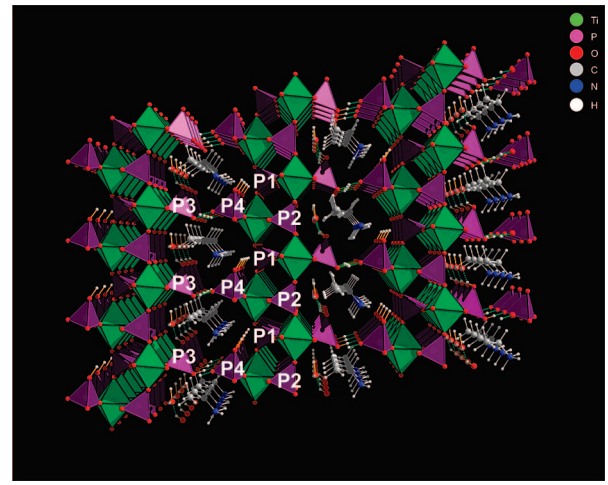

Figure 4. Crystal packing of $(C_2H_5NH_3)[Ti(H_{1.5}PO_4)(PO_4)]_2\cdot H_2O$ represented by a mixed ball-and-stick (guest molecules) and polyhedral (inorganic sheet) representation, viewed along the *a*-axis. Hydrogen bondings are depicted as green dotted lines. The four crystallographically distinct P sites are represented on the figure.

(31) Chen, C.; Yang, Y. L.; Huang, K. L.; Sun, Z. H.; Wang, W.; Yi, Z.; Liu, Y. L.; Pang, W. Q. *Polyhedron* **2004**, *23*, 3033.
(32) Serre, C.; Taulelle, F.; Ferey, G. *Solid State Sci.* **2001**, *3*, 623.
(33) Sung, H. H.-Y.; Yu, J.; Williams, I. D. *J. Solid State Chem.* **1998**, *140*, 46.

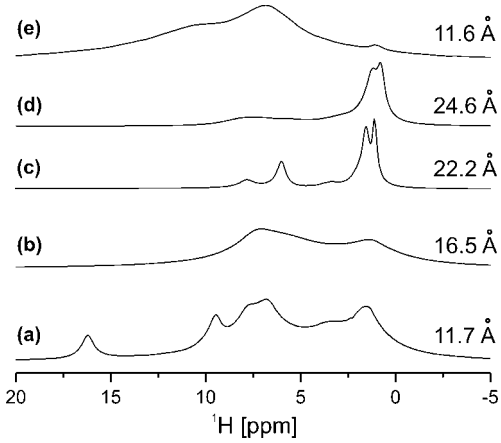

Figure 5. ^{1}H MAS spectra for several γ-TiP/*n*-alkylamine intercalation compounds: (a) $(C_2H_5NH_3)[Ti(H_{1.5}PO_4)(PO_4)]_2\cdot H_2O$, (b) $(C_2H_5NH_3)[Ti(HPO_4)(PO_4)]\cdot 0.3(C_2H_5NH_3)\cdot H_2O$, (c) $(C_6H_{13}NH_3)[Ti(HPO_4)(PO_4)]\cdot H_2O$, (d) $(C_6H_{13}NH_3)[Ti(HPO_4)(PO_4)]\cdot 0.3(C_6H_{13}NH_2)\cdot H_2O$, and (e) γ-TiP.

Scheme 2. Fragment of the $(C_2H_5NH_3)[Ti(H_{1.5}PO_4)(PO_4)]_2\cdot H_2O$ Crystal Structure

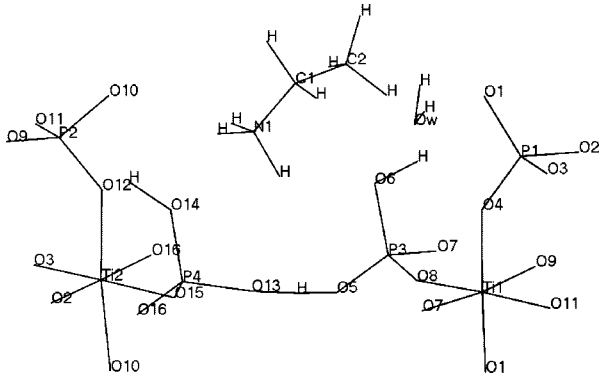

The ^{1}H MAS spectrum of $(C_2H_5NH_3)[Ti(H_{1.5}PO_4)(PO_4)]_2\cdot H_2O$ (Figure 5a) exhibits, between 0−10 ppm, several peaks and shoulders. An unexpected ^{1}H resonance at approximately 16.2 ppm is probably due to hydrogen atoms involved in strong hydrogen-bonding or in a highly acidic ^{1}H environment. The ^{1}H MAS NMR spectra of the different γ-TiP type layered intercalation materials (Figure 5b−e) do not display the 16.2 ppm peak. Because all these materials also contain amine groups close to POH groups, this resonance is presumably not due to the formation of strong hydrogen bonding between the amine and the hydrogenophosphate groups. Consideration of the interlayer *d* spacings suggests that only the basal spacing of $(C_2H_5NH_3)[Ti(H_{1.5}PO_4)(PO_4)]_2\cdot H_2O$ is consistent with a hydrogen-bonding distance, across the gap, between the POH groups of the γ-titanium phosphate sheets ($d_{O5-O13} = 2.43$ Å, Scheme 2). Thus, the inorganic layers may be connected through interlayer PO···H···OP hydrogen bondings. However, $Ti(H_2PO_4)(PO_4)\cdot 2H_2O$, which has a similar basal spacing (11.6 Å, Figure 2e), does not display the 16.2 ppm peak, and, so, additional NMR studies are required to understand its assignment.

^{13}C NMR longitudinal relaxation studies in the laboratory (T_1^C) and rotating ($T_{1\rho}^C$) frames were also conducted (Experimental Section and Table 6). The N−CH_2 groups (ca. 25 s and 85.5 ms, respectively) of $(C_2H_5NH_3)[Ti(H_{1.5}PO_4)(PO_4)]_2\cdot H_2O$ exhibit the longest T_1^C and $T_{1\rho}^C$ values. Due to the intrinsic mobility of CH_3 groups, the interpretation of its relaxation data is not straightforward. Altogether, the relaxation data reveal that the mobility of the ethylamine molecule is considerably reduced in the interlayer space of $(C_2H_5NH_3)[Ti(H_{1.5}PO_4)(PO_4)]_2\cdot H_2O$, presumably because of the presence of the strong PO···H···OP hydrogen bonding networks (perhaps compounded by interactions with other ethylamine molecules).

Table 6. ^{13}C Spin Lattice Relaxation Data in the Laboratory and Rotating Frames for Selected γ-TiP/*n*-Alkylamine Intercalation Compounds

	T_1^C [s]		$T_{1\rho}^C$ [ms]	
compound	N−CH_2	CH_3	N−CH_2	CH_3
$(C_6H_{13}NH_3)[Ti(HPO_4)(PO_4)]\cdot 0.3(C_6H_{13}NH_2)\cdot H_2O$	0.6	1.6	29.8	43.9
$(C_6H_{13}NH_3)[Ti(HPO_4)(PO_4)]\cdot H_2O$	0.4	0.42	2.3	26.2
$(C_2H_5NH_3)[Ti(HPO_4)(PO_4)]\cdot 0.3(C_2H_5NH_3)\cdot H_2O)$	1.2	0.5	4.9	16.7
$(C_2H_5NH_3)[Ti(H_{1.5}PO_4)(PO_4)]_2\cdot H_2O$	25.2	0.9	85.5	124.2

To improve the ^{1}H resolution in the 0−10 ppm region of the $(C_2H_5NH_3)[Ti(H_{1.5}PO_4)(PO_4)]_2\cdot H_2O$ ^{1}H MAS spectrum, (Figure 5a), a 2D ^{1}H{FSLG}-^{1}H homonuclear correlation (HOMCOR) spectrum was performed (Figure 6a). The pertinent ^{1}H MAS spectrum recorded at $\nu_R = 30$ kHz (Figure 6b) is also shown for comparison. Figure 6 reveals the presence of six ^{1}H resonances. The peaks resonating at approximately 1.6 (H^F) and approximately 3.2 (H^E) ppm are assigned to, respectively, CH_3 and CH_2 groups and are also given by the other materials in Figure 5. The remaining ^{1}H peaks at approximately 16.2, 9.4, 7.6, and 6.8 ppm (H^{A-D}) must be assigned to the NH and OH (−POH or H_2O) groups because no other hydrogen containing functional groups are present. These resonances appearing at >6 ppm suggest the occurrence of hydrogen bonding networks or protonated species. Indeed, according to Ratcliffe et al.,[35] hydrogen-bonded protonated water (H_3O^+, $H_5O_2^+$) may resonate at 10.4 to 18.1 ppm. In addition, P−OH and NH groups with different hydrogen-bonding strengths may also overlap in this region, further complicating the spectral interpretation.

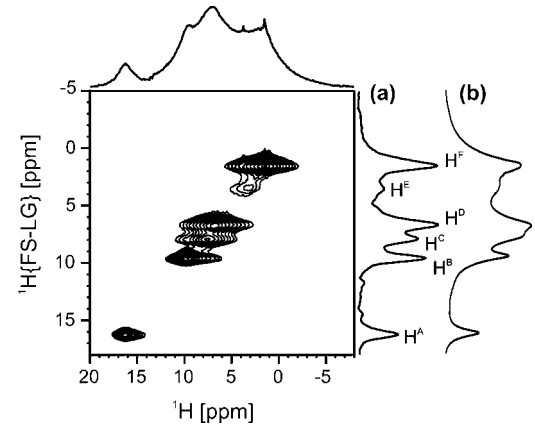

Figure 6. (a) 2D ^{1}H{FS-LG}-^{1}H HOMCOR and (b) ^{1}H fast MAS NMR spectra of $(C_2H_5NH_3)[Ti(H_{1.5}PO_4)(PO_4)]_2\cdot H_2O$.

(34) Harris, R. K.; Merwin, L. H.; Hagele, G. *Magn. Reson. Chem.* **1989**, *27*, 470.

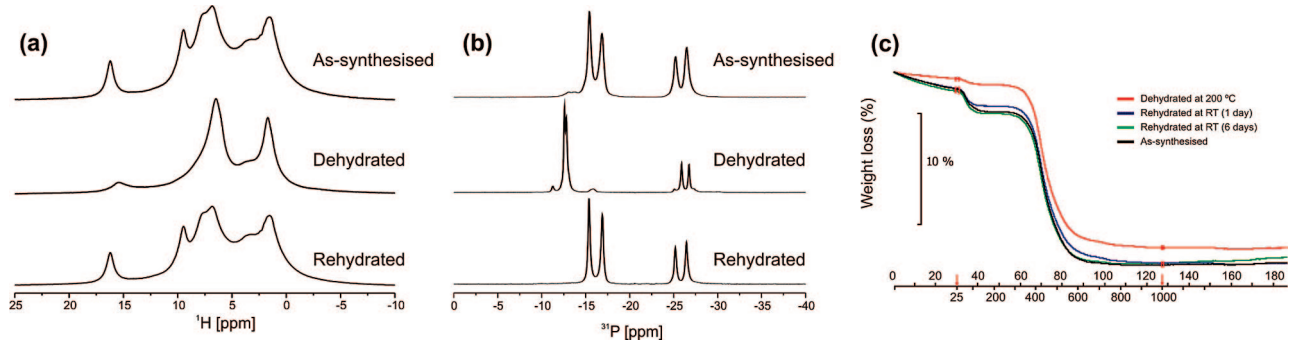

Figure 7. Dehydration−hydration process of $(C_2H_5NH_3)[Ti(H_{1.5}PO_4)(PO_4)]_2 \cdot H_2O$: (a) ^{1}H MAS, (b) ^{31}P CPMAS NMR, and (c) TGA.

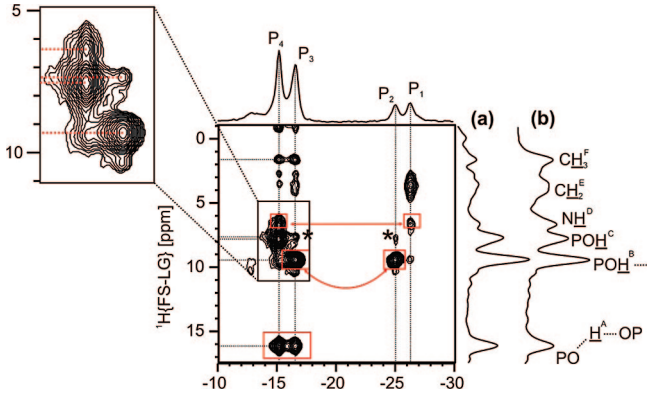

Figure 8. 2D ^{1}H{FS-LG}-^{31}P HETCOR NMR spectrum of $(C_2H_5NH_3)[Ti(H_{1.5}PO_4)(PO_4)]_2 \cdot H_2O$ employing CTs of (a) 0.1 ms and (b) 1 ms.

The dehydration and rehydration experiments (Figure 7a−c) have shown that in $(C_2H_5NH_3)[Ti(H_{1.5}PO_4)(PO_4)]_2 \cdot H_2O$ the water loss is reversible. Upon dehydration, the ^{1}H peak at approximately 9.4 ppm (H^B) disappears, while the other resonances are essentially not affected (Figure 7a). This resonance may be assigned to either POH groups hydrogen-bonded to water molecules or, less likely, to the hydronium cation protons (which may, in principle, be present).[35] Although dehydration does not much change the ^{31}P NMR resonances of the orthophosphate groups (P1 and P2 sites), there is a considerable high-frequency shift of hydrogenophosphate (P3 and P4 sites) peaks (Figure 7b).

Consider the 2D ^{1}H{FSLG}-^{31}P HETCOR experiment (Figure 8). The ^{1}H-^{31}P correlations allow the unambiguous assignment of the ^{1}H nuclei close to the ^{31}P nuclei. To avoid the effects of strong ^{1}H-^{1}H dipolar couplings, which may deteriorate the spectral resolution and the CP coherence transfer selectivity, FSLG during t_1 evolution with LG-CP or very short CP mixing times was employed. These ^{1}H decoupling schemes quench ^{1}H-^{1}H spin diffusion affording information on the ^{1}H-^{31}P spin pairs close in space. 2D ^{1}H{FSLG}-^{31}P HETCOR (Figure 8) clearly shows that the 16.2 ppm ^{1}H resonance (H^A) is correlated to both hydrogenophosphate (P3 and P4 sites) peaks. We discard the, in principle, possible assignment of this peak to hydrogen bonding between the ethyamine NH and γ-Ti phosphate layer POH groups for the following reasons. First, according to Figure 8a, the two crystallographically distinct POH sites (P3 and P4) reside in opposite sides of the γ-Ti phosphate sheets (see Scheme 2). Second, if the ethylamine molecules are aligned perpendicularly, in a nonalternated fashion (i.e., ethylamine molecules are all oriented in the same direction), with respect to the γ-Ti phosphate layers, with the polar head pointing to one of these sheets, only one ^{31}P site (P3 or P4) should have a strong cross peak with H^A in the HETCOR spectrum. In addition, if the ethylamine residues were alternated between an up and down arrangement, all the hydrogenophosphate P3 and P4 ^{31}P sites would be crystallographically equivalent. The same situation happens if the intercalated alkylamine adopts a bilayer arrangement.[6] In addition, the cross-peaks between H^A and P3 and P4 are very intense, indicating that the distances between these protons and phosphorus atoms are similar. In summary, ^{1}H{FSLG}-^{31}P HETCOR spectra indicate the presence of strong hydrogen-bonding (P3)O···H^A···O(P4) (Figure 4). In O-phophorylated amino acids PO···H···OP hydrogen bonding ^{1}H peaks may occur above 16 ppm, thus encompassing the 16.2 ppm found in our work.[36] We recall that modeling of the $(C_2H_5NH_3)[Ti(H_{1.5}PO_4)(PO_4)]_2 \cdot H_2O$ X-ray diffraction pattern shows that the O···O distance in PO(5)···H···O(13)P is approximately 2.4 Å, in accord with the reported O-phosphorylated amino acids data.[36]

H^B and H^D protons have strong cross-peaks only with, respectively, P2 and P3, and P1 and P4 phosphorus. Therefore, because P3 and P4 are POH groups residing on opposite sides of the inorganic sheet, H^B and H^D must be also located in opposed sides of the inorganic layer, according to ^{1}H-^{31}P contacts (Figure 8). Thus, H^D is assigned to NH protons with the ethylamine polar head residing between POH (P4) groups (Figure 4). Moreover, the chemical shift of H^D (ca. 6.8 ppm) is typical of protonated NH groups. This assignment is also supported by the presence of a single cross-peak between the N−CH_2 group protons (H^E) and P1 (PO_4 groups, Figure 8a), supporting that the polar part of the ethylamine molecules is interpenetrating the inorganic γ-Ti phosphate layers.

The H^C resonance is probably the most difficult to assign: it may be given by water molecules and/or P4-OH group. Indeed, a strong cross-peak is observed between H^C and P4, while faint peaks are also seen between H^C and P2 and P3 (Figure 8) which, supposedly, are closer to the water

(35) Ratcliffe, C. I.; Ripmeester, J. A.; Tse, J. S. *Chem. Phys. Lett.* **1985**, *120*, 427.
(36) Potrzebowski, M. J.; Assfeld, X.; Ganicz, K.; Olejniczak, S.; Cartier, A.; Gardiennet, C.; Tekely, P. *J. Am. Chem. Soc.* **2003**, *125*, 4223.
(37) d'Antuono, P.; Botek, E.; Champagnea, B.; Spassova, M.; Denkova, P. *J. Chem. Phys.* **2006**, *125*, 144309.

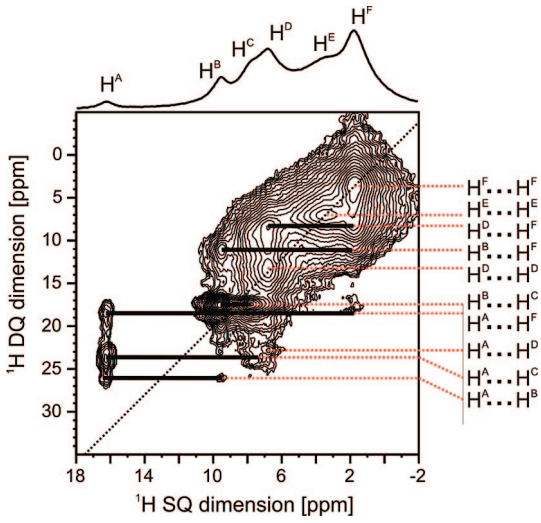

Figure 9. 2D ^{1}H-^{1}H DQ-SQ MAS spectrum of $(C_2H_5NH_3)[Ti(H_{1.5}PO_4)(PO_4)]_2 \cdot H_2O$.

molecules (Figure 4), because the H^B resonance, assigned to P−OH hydrogen-bonded to water molecules, also displays cross-peaks with the same phosphorus sites. In addition, water may be in fast exchange with POH groups.

To further confirm the assignment ^{1}H NMR spectra, chemical shifts were calculated by DFT using the GIPAW method, using the molecular species shown in Scheme 1 $[(H_3PO_4)(H_2PO_4)]^-$ and $NH_4H_2PO_4$. Considering the calculated isotropic chemical shift values given in Table 4, the attribution of H^A and H^{B-D} protons is unambiguous. The calculated H^A chemical shifts of $[(H_3PO_4)(H_2PO_4)]^-$ and $NH_4H_2PO_4$ are, respectively, 18.2 and 15.3 ppm, in good agreement with the experimental value of 16.2 ppm. Hence, DFT calculations do support the existence of strong interlayer hydrogen bonds. The calculated and experimental H^{B-D} chemical shifts are also in fair accordance (Table 4).

To probe ^{1}H-^{1}H distances we have used a ^{1}H homonuclear recoupling experiment,[20] where the coupled ^{1}H spins which appear at the sum of their chemical shifts along the double-quantum (DQ) frequency dimension are correlated with the single-quantum (SQ) coherences (Figure 9). This experiment has the ability to filter mobile molecules and weakly dipolar coupled ^{1}H resonances. The ^{1}H DQ-SQ spectrum of as-prepared $(C_2H_5NH_3)[Ti(H_{1.5}PO_4)(PO_4)]_2 \cdot H_2O$ (Figure 9) shows all the peaks present in the ^{1}H MAS spectrum (Figure 5a). This indicates that the ^{1}H network is relatively rigid, and, thus, the ^{1}H cross-peaks intensity is mainly affected by the ^{1}H-^{1}H distance. Peaks along the diagonal are observed for CH_3 ($H^F \cdots H^F$) and CH_2 ($H^E \cdots H^E$) protons, due to the presence of geminal protons on such carbon atoms. Moreover, H^D also present a DQ peak ($H^D \cdots H^D$) at approximately 13.6 ppm, which supports their assignment to NH protons, as stated before, because there is more than one hydrogen atom attached to the nitrogen atom that may originate double-quantum transitions. In contrast, and in accord with the crystal model, H^A protons do not display any peaks along the diagonal, which shows that, in a given γ-titanium phosphate sheet, the shortest P···P distance between adjacent P−OH groups is 5.1−6.3 Å (Figure 3a,d). This is expected because the SQ-DQ experiment detects ^{1}H-^{1}H shorter than

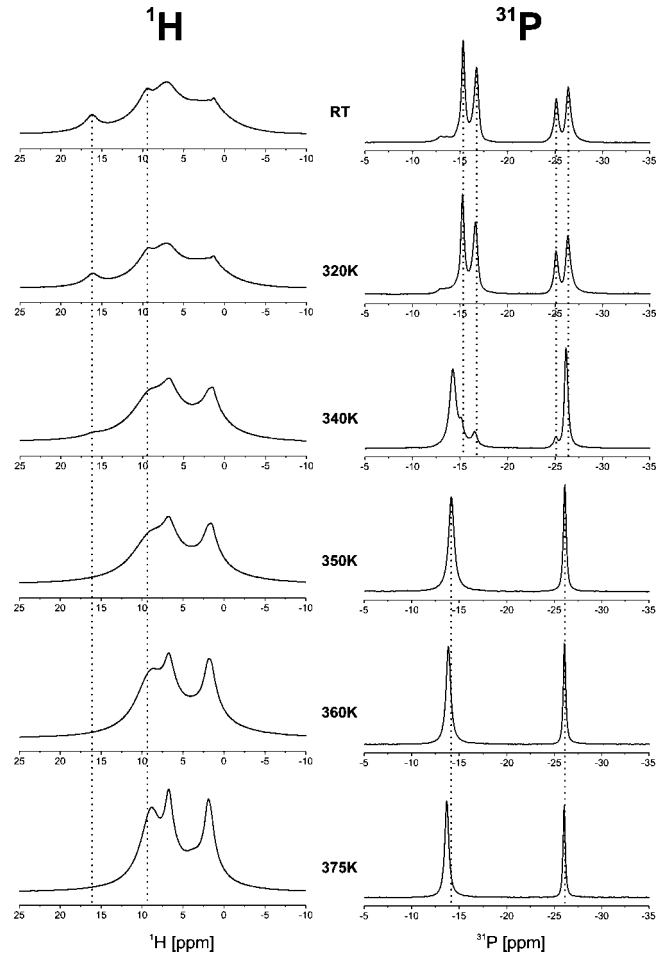

Figure 10. Variable temperature measurements of (a) ^{1}H MAS and (b) ^{31}P CPMAS spectra.

approximately 3.5 Å. Since P3,4-OH has only a single ^{1}H attached, no diagonal peaks are expected, and it is indeed so. H^B also has one off-diagonal DQ peak ($H^B \cdots H^F$) at approximately 11 ppm, indicating its proximity to CH_3 protons, as revealed by X-ray data.

Variable Temperature Measurements. We have followed the effect of the temperature on the 16.2 ppm peak (strong hydrogen bonding) by ^{1}H MAS NMR (Figure 10). At 350 K this peak is no longer observed, indicating that the strong hydrogen-bonding network has been disrupted. Simultaneously, the ^{31}P CPMAS NMR spectra change from four to two crystallographically distinct ^{31}P sites (Figure 10). This gain in symmetry, which makes the P3 and P4 sites equivalent, is probably brought about by the larger molecular mobility of the guest molecules at higher temperature.

Study of Ethylamine Orientation by ^{13}C-{^{31}P} REDOR. Making use of the $^{13}C \cdots ^{31}P$ dipolar couplings, we have attempted to obtain information on the molecular orientation of the ethylamine residues relative to the γ-titanium phosphate sheets. For this purpose, the REDOR method was employed. Specifically, the distances between the ^{13}C ethylamine and the ^{31}P spins located on the surface of the 2D $[Ti(HPO_4)(PO_4)]^-$ sheets were assessed by REDOR. Figure S5, Supporting Information, shows an acceptable fitting only for the initial points (up to ca. 4 ms) of the CH_2 and CH_3 curves. This feature is typical of multiple-spin couplings in solids. Because the interlayer space is small

Table 7. Experimental Principal Values[a] of the ^{31}P CSA Tensor of the POH Groups in γ-TiP/Ethylamine Intercalation Compounds

compound	phosphorus group	δ_{iso} (ppm)	δ_{11} (ppm)	δ_{22} (ppm)	δ_{33} (ppm)	δ_{aniso} (ppm)	Ω (ppm)	κ	η
$(C_2H_5NH_3)[Ti(H_{1.5}PO_4)(PO_4)]_2 \cdot H_2O$	P_3-OH	−16.8	24.1	−10.6	−63.9	−47.1	88.0	0.21	0.74
	P_4-OH	−15.4	15.8	−23.5	−38.5	31.2	54.3	−0.45	0.48
$(C_2H_5NH_3)[Ti(H_{1.5}PO_4)(PO_4)]_2$	P−OH[b]	−12.5	25.1	−19.9	−42.6	37.6	67.7	−0.33	0.60

[a] Estimated errors in δ_{11}, δ_{22}, and δ_{33} are ±3 ppm; span is expressed as $\Omega = \delta_{11} - \delta_{33} > 0$, and anisotropy is calculated as $\delta_{aniso} = (\delta_{33} - \delta_{iso})$ and asymmetry as $\eta = (\delta_{22} - \delta_{11})/(\delta_{33} - \delta_{iso})$ when $|\delta_{11} - \delta_{iso}| \leq |\delta_{33} - \delta_{iso}|$ or as $\delta_{aniso} = (\delta_{11} - \delta_{iso})$ and $\eta = (\delta_{22} - \delta_{33})/(\delta_{11} - \delta_{iso})$ when $|\delta_{11} - \delta_{iso}| \geq |\delta_{33} - \delta_{iso}|$; skew is expressed as $\kappa = 3(\delta_{22} - \delta_{iso})/\Omega$, $(-1 \leq k \leq +1)$. [b] The dehydrated sample contains two distinct POH ^{31}P resonances almost coincident (data not shown) and could not be separated to adequately calculate the CSA values for each ^{31}P site. Therefore, the presented values are the average contribution of both POH sites.

and many ^{31}P nuclei surround each ^{13}C atom (Figure 4), measuring a single distance for a given $^{13}C-^{31}P$ spin pair is not possible. However, if only the first data points are considered, the minimum C−P distance may be estimated for CH_2 and CH_3 groups. The results taken from the curve fitting shows a minimum C−P distance of about 3.7−3.8 Å (D_{ij} = 223−242 Hz), which is in accord with the crystal structure. The REDOR experiment was also used in other γ-TiP intercalates (Figure S6, Supporting Information), clearly showing that the $^{13}CH_3$ of $(C_2H_5NH_3)[Ti(HPO_4)(PO_4)] \cdot 0.3(C_2H_5NH_2) \cdot H_2O$ dephases slowly, relatively to that of $(C_2H_5NH_3)[Ti(H_{1.5}PO_4)(PO_4)]_2 \cdot H_2O$, supporting the view that the former adopts a bilayer structure for the organic guest. The data also show that the longer the alkylamine chain is the slower the $^{13}CH_3$ dephasing is, because the CH_3 groups become more distant from the layer surface. Moreover, the $N-^{13}CH_2$ peaks dephase with almost the same rate, because the $N-CH_2$ groups of the different γ-TiP intercalates have their polar part directed toward the layers. Thus, the $P\cdots CH_2-N$ distances are similar for all materials. The results obtained by comparing different materials in the same family indicate that the $^{13}C-^{31}P$ REDOR curve fitting procedure used here yields an approximate value for the minimum C−P distance in $(C_2H_5NH_3)[Ti(H_{1.5}PO_4)(PO_4)]_2 \cdot H_2O$. The obtained C−P distances were, hence, used as input to the XRD modeling studies.

Water Influence on ^{31}P Chemical Shift Anisotropy (CSA). To the best of our knowledge, there are no studies on the influence of dehydration on the eigenvalues of the ^{31}P CSA tensor on host−guest systems, and thus the interpretation of the obtained results is not trivial (Table 7). Moreover, no information is available on the orientation of the ^{31}P CSA tensor with respect to the principal molecular frame, which is needed to discuss the results. Nevertheless, CSA parameters were extracted from the ^{31}P CPMAS spinning-sideband manifold (Figure S7, Supporting Information). A comparison of the principal values of the ^{31}P CSA tensor of as-synthesized and dehydrated $(C_2H_5NH_3)[Ti(H_{1.5}PO_4)(PO_4)]_2 \cdot H_2O$ reveals that the P−OH and P(4)−OH δ_{22} and δ_{33} values are similar (difference < 4 ppm). Considering the anisotropy (δ_{aniso}), the difference between the samples is approximately 6 ppm for the P(4)−OH sites and approximately 85 ppm for the P(3)−OH sites. The Ω values, which characterize the maximum width of the powder pattern, of P−OH and P(4)−OH are not too different and much smaller than the P(3)−OH value (Table 7). The skew κ of the tensor is positive for P−OH and P(4)−OH but negative for P(3)−OH. In summary, the analysis of the ^{31}P NMR CSA parameters suggests that the water molecules should be located close to the P(3) sites, the most affected upon dehydration, in accord with the $^{1}H\{FSLG\}-^{31}P$ HETCOR experiment.

Conclusion

Layered γ-titanium phosphates intercalated with alkylamine molecules have been studied by synchrotron powder X-ray diffraction in tandem with high-resolution NMR spectroscopy, particularly ^{1}H CRAMPS techniques, which provide insight into the local environment of the ^{1}H nuclei. Key to the full elucidation of the structure of the materials was the combination of XRD and NMR evidence with theoretical calculations of ^{1}H NMR chemical shifts using the GIPAW approach available in the CASTEP-NMR package. In this way, and in particular, it was possible to (i) assign all ^{1}H NMR resonances; (ii) identify an unusual strong hydrogen bond bridging between the γ-titanium phosphate layers; and (iii) establish the location/orientation of the guest alkylamine molecules in the interlayer space.

Acknowledgment. We are grateful for financial support from FEDER and Fundação para a Ciência e Tecnologia (FCT). We are also grateful to Conselho de Reitores das Universidades Portuguesas (CRUP) for funding (Acção No. E-93/08, Proc. AI-E/07) [Portugal]. We acknowledge the Spanish Ministerio de Educación y Ciencia (MAT2006-01997 and Factoría de Cristalización − Consolider Ingenio 2010) and Gobierno del Principado de Asturias (PCTI 2006-2009). The authors also thank SpLine beamline staff for support during the powder XRD experiments and the financial support from MEC and the CSIC (Intramural 2004 5 OE 292) for the realization of the powder synchrotron XRD experiments.

Supporting Information Available: TG-DTG-DSC curves, TEM image, FTIR spectrum, and MAS NMR data (^{13}C and ^{15}N CPMAS, and experimental and theoretical ^{31}P CPMAS spectra) of $(C_2H_5NH_3)[Ti(H_{1.5}PO_4)(PO_4)]_2 \cdot H_2O$. Comparison of CH_3 and $N-CH_2$ ^{13}C REDOR curves for γ-TiP type intercalated compounds.

CM800165P